

Mechanical Buckling Analysis of Composite Annular Sector Plate with Bean-Shaped Cut-Out using Three Dimensional Finite Element Method

H. Behzad¹, A.R. Shaterzadeh^{1,*}, M. Shariyat²

¹*Faculty of Mechanical Engineering, Shahrood University of Technology, Shahrood, Iran*

²*Faculty of Mechanical Engineering, K.N. Toosi University of Technology, Tehran, Iran*

Received 30 March 2018; accepted 27 May 2018

ABSTRACT

In this paper, mechanical buckling analysis of composite annular sector plates with bean shape cut out is studied. Composite material sector plate made of Glass-Epoxy and Graphite-Epoxy with eight layers with same thickness but different fiber angles for each layer. Mechanical loading to form of uniform pressure loading in radial, environmental and biaxial directions is assumed. The method used in this analysis is three dimensional (3D) finite elements based on the elasticity relations. With zero first and second variation of potential energy of the entire annular sector plate, we find stability equation. Green non-linear displacement strain relations to obtain geometric stiffness matrix is used. Unlike many studies, in present work three dimensional finite elements method has been used with an eight node element and meshing in the thickness direction is done, too. The bean shaped cut out in the sector has increased the complexity of the analysis. The continuing, effect of different parameters including cut out dimensions, fiber angles of layers, loading direction and dimensions of the annular sector plate on the mechanical buckling load has been investigated and interesting results have been obtained. © 2018 IAU, Arak Branch. All rights reserved.

Keywords : Annular sector plate; Composite material; 3D finite elements method; Mechanical buckling.

1 INTRODUCTION

ANNULAR sector plates have wide application in industry such as parts used in automobile, building, industry, etc. That is why studying and analyzing the behavior of these plates is important. Plates are affected by in-plane compression loading during application which creates buckling in the plate. Therefore, one of the important parameters for plate designing is investigation of the buckling behavior. Buckling may occur due to applying different loadings such as mechanical, thermal loadings, etc. Therefore, analysis of mechanical buckling perforated plate with annular sector geometry will be presented in this paper. The plate is made of composite material due to its various advantages; some of them are light weight, good resistance against corrosion and fatigue, high elasticity module and high overall resistance with low density. These are the reasons why composite materials are used in engineering and industries such as aerospace, automobile and building industry, and etc. Using precise solution makes the structure modeling complicated as well as giving exact answer and it is not developed enough to

*Corresponding author.

E-mail address: a_shaterzadeh@shahroodut.ac.ir (A.R. Shaterzadeh).

cover structures with different conditions. Thus, using numerical methods with acceptable error in the final answer and also a variety of analyzing structures with different conditions is more common. Finite element method (FEM) based on three-dimensional (3D) elasticity theory is used in this paper. Thick plates can be analyzed using 3D elasticity theory in analogy with other plate theories. The following studies have investigated plate buckling with conditions similar to this analysis.

Bruno and Lato [1] studied the buckling of thick composite plates. Chai [2] presented the buckling of laminated composite plates with different boundary conditions on edges. Kim and Hoa [3] studied buckling behavior of rectangular composite plates. Zhou et al., [4] proposed a semi-scalar method for the buckling of sector plates. Sundaresan et al., [5] studied the buckling of thick rectangular composite plates which part of edges was under compressive loading. Shariyat [6] analyzed thermal buckling of rectangular composite with thermal-dependent characteristics using layer wise theory. Özben [7] studied critical-load buckling of laminated composite plates with different boundary conditions using finite element scalar method and analytical method. Alipour and Shariyat [8] proposed semi-analytic solution for buckling of heterogeneous viscoelastic circular plates in elastic foundations. Dash and Singh [9] studied buckling and post-buckling of laminar composite plate. Jabbarzadeh and Baghdar [10] analyzed thermal buckling of sector plate made of Functionally Graded Materials (FGM) using Differential Quadrature Method (DQM). Asemi and Shariyat [11] presented non-linear 3D finite element method with high precision for biaxial buckling of rectangular anisotropic plates. Fazzolari et al., [12] analyzed buckling of composite plates using higher order shear deformation plate theory (HSDT) and exact method of solution. Lopatin and Morzov [13] presented buckling of rectangular composite plate under monotonous compressive loading. Asemi et al., [14] presented post-buckling behavior of annular sector plates made of Functionally Graded Material using simply supported conditions under compressive loading. Abolghasemi et al., [15] studied buckling of rectangular functionally graded plate with elliptic cutout. Nasirmanesh and Mohammadi [16] analyzed cracked composite plate buckling using finite element method. Rezaei et al., [17] presented the buckling of rectangular plate made of functionally graded material with elliptic cutout under thermal loading. Shaterzadeh [18] performed thermomechanical buckling of functionally graded plates with circular cutout on the center. Mansouri and Shariyat [19] performed thermomechanical buckling of functionally graded plates with thermal-dependent characteristics on elastic foundation.

Studying the buckling of sector plate is more difficult due to geometric condition and few researches are attributed to annular sector plates. It is attempted to study the mechanical buckling of sector plates with bean-shaped cutout with 3D finite element method.

2 CONDITIONS

2.1 Geometry of sector plates

Considering the geometry of annular sector plate and its bean-shaped cutout, the best coordinate system for describing its geometry is cylindrical coordinate system in which three values of diameter, r , angle, θ , and thickness, z , of the sector should be determined. If a , b , h , and β are internal, external diameters, thickness, and angle of the sector, respectively, cylindrical coordinate system should be established so that:

$$b \leq r \leq a, 0 \leq \theta \leq \beta, -\frac{h}{2} \leq z \leq \frac{h}{2}$$

A bean-shape opening should be cutout in the sector, according to Fig. 1, to investigate the effect of opening on buckling strength of the annular sector. Bean-shape opening of the sector can be described with two parameters of origin coordination, radial and circumferential variations of the opening. We consider the opening so that it would be symmetrical in r and θ direction; therefore, center of the sector opening will always have coordination of $r_c = (a+b)/2$ and $\theta_c = \beta/2$ in this paper. Variations of cutout diameter ($r_2 - r_1$) express cutout size in r axis direction and circumferential variations of cutout ($\theta_2 - \theta_1$) are cutout size in θ axis direction. Also, depth of the cutout equals sector thickness.

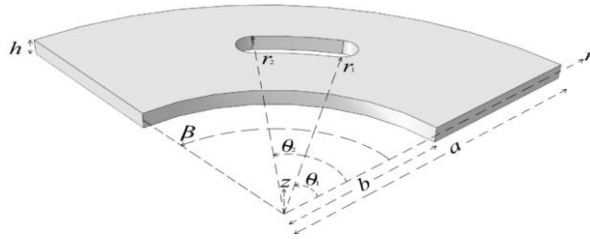


Fig.1
Geometry of the sector plate.

2.2 Method of loading

Mechanical loading is considered in three states of uniform compressive loading in radial, circumferential and combined (biaxial) directions under radial and circumferential loading to study the effect of load direction on buckling results. Fig. 2 shows sector plate with biaxial loading.

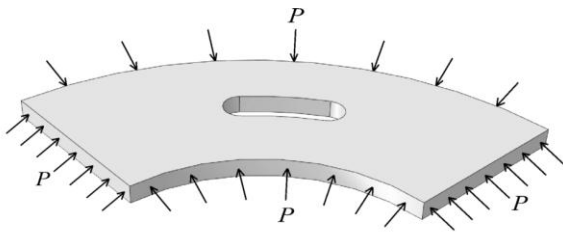


Fig.2
Schematic of biaxial loading.

Loading conditions for mentioned loading modes given in Table1. p is the applied load to faces of sector.

Table 1
Method of compressive loading on annular sector plate.

Loading direction	Right surface ($\theta = 0$)	left surface ($\theta = \beta$)	inner surface ($r = b$)	outer surface ($r = a$)
Radial	without loading	without loading	radial loading	radial loading
Circumferential	circumferential loading	circumferential loading	without loading	without loading
Biaxial	circumferential loading	circumferential loading	radial loading	radial loading

2.3 Kinematic conditions

Natural boundary conditions (such as moment, shear force, and compressive load in edge) have been applied in functional form. Kinematic conditions for various loading are addressed in Table 2. u_t, u_n is tangential and normal displacements to surface of sector, respectively. It should be noted that displacement of boundaries in thickness direction is zero.

Table 2
Kinematic conditions of annular sector plate.

Loading direction	Right surface ($\theta = 0$)	left surface ($\theta = \beta$)	inner surface ($r = b$)	outer surface ($r = a$)
Radial	$u_t, u_n = 0$	$u_t, u_n = 0$	$u_t = 0$	$u_t = 0$
Circumferential	$u_t = 0$	$u_t = 0$	$u_t, u_n = 0$	$u_t, u_n = 0$
Biaxial	$u_t = 0$	$u_t = 0$	$u_t = 0$	$u_t = 0$

2.4 Sector material

Sector is made of composite material considered in 8 layers in the thickness direction and layers are arranged symmetrically regarding the main coordination system. Thickness of the layers is similar and equals $h/8$. Layer arrangement is assumed in two cases of $[0, 90]_4$ and $[45, -45]_4$ so that its effect on buckling loading can be studied.

It is assumed that two upper and lower layers are made of Graphite-Epoxy composite and four middle layers of Glass-Epoxy. Characteristics of these two composite materials are expressed in Table 3. [21]

Table 3
Material properties of Graphite-Epoxy & Glass-Epoxy [21].

Properties	Material	
	Graphite-Epoxy (T300/5208)	Glass-Epoxy (s-2)
$E_1 [N/m^2]$	132×10^9	43.5×10^9
$E_2 [N/m^2]$	10.8×10^9	11.5×10^9
$G_{12} [N/m^2]$	5.65×10^9	3.45×10^9
$G_{23} [N/m^2]$	3.38×10^9	4.12×10^9
ν_{12}	0.24	0.27
ν_{23}	0.59	0.4

3 FORMULATION

3.1 3D Elasticity theory

The governing equations are defined from Lagrangian description point of view in reference coordination system or un-deformed configuration [22].

Elasticity relations of the plate with mentioned geometry are expressed firstly in cylindrical coordination system.

3.1.1 Stress- strain relations

Stress-strain relation can be expressed for k^{th} layer based on Hook's law considering the sector is made of 8-layer composite, as shown below:

$$\{\sigma\}^{(k)} = [D]^{(k)} \{\varepsilon\}^{(k)} \quad (1)$$

which σ is stress vector and ε is strain vector and each one is expressed in cylindrical coordination system as follows:

$$\{\sigma\} = [\sigma_{rr} \quad \sigma_{\theta\theta} \quad \sigma_{zz} \quad \tau_{r\theta} \quad \tau_{\theta z} \quad \tau_{rz}]^T \quad (2)$$

$$\{\varepsilon\} = [\varepsilon_{rr} \quad \varepsilon_{\theta\theta} \quad \varepsilon_{zz} \quad \gamma_{r\theta} \quad \gamma_{\theta z} \quad \gamma_{rz}]^T \quad (3)$$

Elasticity matrix for k^{th} layer is stated as follow:

$$[D] = \begin{bmatrix} \bar{Q}_{11} & \bar{Q}_{12} & \bar{Q}_{13} & \bar{Q}_{16} & 0 & 0 \\ & \bar{Q}_{22} & \bar{Q}_{23} & \bar{Q}_{26} & 0 & 0 \\ & & \bar{Q}_{33} & \bar{Q}_{36} & 0 & 0 \\ & & & \bar{Q}_{66} & 0 & 0 \\ \text{sym.} & & & & \bar{Q}_{44} & \bar{Q}_{45} \\ & & & & & \bar{Q}_{55} \end{bmatrix} \quad (4)$$

\bar{Q}_{ij} depends on the material and orientation of fiber angles. For more information about this topic refer to [21, 23]. In addition, as fiber angles are expressed in relation to Descartes axis, elasticity matrix can be obtained using transform matrix.

3.1.2 Strain- displacement relation

As shape variation in relation to loading increment is disproportionate at the moment of buckling, Green’s strain-displacement relation should be used which includes linear relation of strain-displacement before buckling and also non-linear relation of strain-displacement at the moment of buckling.

Strain-displacement relation can be decomposed as the two sections of linear and non-linear part

$$\{\varepsilon\} = \{\varepsilon_L\} + \{\varepsilon_{NL}\} \tag{5}$$

If we show displacement in three main directions as u , v , and w , respectively, then we can state linear and non-linear parts of strain-displacement part as follows:

$$\{\varepsilon_L\} = \left[u_{,r} \quad \frac{u + v_{,\theta}}{r} \quad w_{,z} \quad \frac{u_{,\theta} - v}{r} + v_{,r} \quad v_{,z} + \frac{w_{,\theta}}{r} \quad u_{,z} + w_{,r} \right]^T \tag{6}$$

$$\{\varepsilon_{NL}\} = \begin{bmatrix} \frac{1}{2}(u_{,r}^2 + v_{,r}^2 + w_{,r}^2) \\ \frac{1}{2} \left(\left(\frac{u_{,\theta} - v}{r} \right)^2 + \left(\frac{u + v_{,\theta}}{r} \right)^2 + \left(\frac{w_{,\theta}}{r} \right)^2 \right) \\ \frac{1}{2}(u_{,z}^2 + v_{,z}^2 + w_{,z}^2) \\ u_{,r} \left(\frac{u_{,\theta} - v}{r} \right) + v_{,r} \left(\frac{u + v_{,\theta}}{r} \right) + w_{,r} \left(\frac{w_{,\theta}}{r} \right) \\ u_{,z} \left(\frac{u_{,\theta} - v}{r} \right) + v_{,z} \left(\frac{u + v_{,\theta}}{r} \right) + w_{,z} \left(\frac{w_{,\theta}}{r} \right) \\ u_{,r} u_{,z} + v_{,r} v_{,z} + w_{,r} w_{,z} \end{bmatrix} \tag{7}$$

3.2 Applying FEM

3D 8-noded elements are used to model the sector. Therefore, elements are in the direction of thickness which leads to difference between the current analysis and existing plate theories as traverse displacement of the plate in element will be different. It should be noted that displacement is continuous at the boundary of elements but gradient and consequently strain and stress have no continuity at the boundaries.

If $\{q\}$ and $\{\Delta\}$ are considered displacement vector for any point and arbitrary element nodes, respectively, their relation can be written as follows:

$$\{q\} = [N]\{\Delta\} \tag{8}$$

where

$$\{q\} = [u \quad v \quad w]^T \tag{9}$$

$$\{\Delta\} = [u_1 \quad v_1 \quad w_1 \quad \dots \quad u_8 \quad v_8 \quad w_8]^T \tag{10}$$

Shape function matrix in relation (8) will be as follows:

$$[N] = \begin{bmatrix} N_1 & 0 & 0 & & N_8 & 0 & 0 \\ 0 & N_1 & 0 & \dots & 0 & N_8 & 0 \\ 0 & 0 & N_1 & & 0 & 0 & N_8 \end{bmatrix} \quad (11)$$

Components of shape function matrix for a 3D 8-noded linear element can be obtained from this relation [22].

$$N_i = \frac{1}{8}(1 + \xi\xi_i)(1 + \eta\eta_i)(1 + \zeta\zeta_i) \quad (12)$$

where ξ, η and ζ are right-hand principals of natural coordination system which its range for any element will be as follows:

$$-1 \leq \xi, \eta, \zeta \leq 1$$

The following relation can be considered between components of cylindrical and natural coordination system regarding the geometry of each element [14].

$$\xi = \frac{2r - a^{(e)} - b^{(e)}}{a^{(e)} - b^{(e)}} \quad , \eta = \frac{2(\theta - \theta_c)}{\beta^{(e)}} \quad , \zeta = \frac{2(z - z_c)}{h^{(e)}} \quad (13)$$

In Eq. (13), $a^{(e)}, b^{(e)}, \beta^{(e)}$ and $h^{(e)}$ are internal and external diameter, angle, and thickness of each element, respectively. Also, θ_c and z_c are coordination of each element center in global (cylindrical) coordination system. Linear part of Green's strain relation can be written in this way:

$$\{\varepsilon_L\} = [d_L]\{q\} \quad (14)$$

where

$$[d_L] = \begin{bmatrix} \frac{\partial}{\partial r} & 0 & 0 \\ \frac{1}{r} & \frac{\partial}{r\partial\theta} & 0 \\ 0 & 0 & \frac{\partial}{\partial z} \\ \frac{\partial}{r\partial\theta} & \frac{\partial}{\partial r} - \frac{1}{r} & 0 \\ 0 & \frac{\partial}{\partial z} & \frac{\partial}{r\partial\theta} \\ \frac{\partial}{\partial z} & 0 & \frac{\partial}{\partial r} \end{bmatrix} \quad (15)$$

Replacing Eq. (10) in (14), linear part of strain-displacement relation can be rewritten as follows:

$$\{\varepsilon_L\} = [B_L]\{\Delta\} \quad (16)$$

where linear strain-displacement matrix in cylindrical coordination system equals:

$$[B_L] = \begin{bmatrix} \frac{\partial N_1}{\partial r} & 0 & 0 & \frac{\partial N_8}{\partial r} & 0 & 0 \\ \frac{N_1}{r} & \frac{\partial N_1}{r \partial \theta} & 0 & \frac{N_8}{r} & \frac{\partial N_8}{r \partial \theta} & 0 \\ 0 & 0 & \frac{\partial N_1}{\partial z} & 0 & 0 & \frac{\partial N_8}{\partial z} \\ \frac{\partial N_1}{r \partial \theta} & \frac{\partial N_1}{\partial r} - \frac{N_1}{r} & 0 & \frac{\partial N_8}{r \partial \theta} & \frac{\partial N_8}{\partial r} - \frac{N_8}{r} & 0 \\ 0 & \frac{\partial N_1}{\partial z} & \frac{\partial N_1}{r \partial \theta} & 0 & \frac{\partial N_8}{\partial z} & \frac{\partial N_8}{r \partial \theta} \\ \frac{\partial N_1}{\partial z} & 0 & \frac{\partial N_1}{\partial r} & \frac{\partial N_8}{\partial z} & 0 & \frac{\partial N_8}{\partial r} \end{bmatrix} \quad (17)$$

Similarly, nonlinear part of strain-displacement relation can be expressed as:

$$\{\varepsilon_{NL}\} = [B_{NL}]\{\Delta\} \quad (18)$$

Nonlinear strain-displacement matrix in cylindrical coordination system equals:

$$[B_{NL}] = [B_{NL}^{(1)} \quad \dots \quad B_{NL}^{(8)}] \quad (19)$$

As element terms of nonlinear strain- displacement matrix are lengthy, it can be shown as relation (20):

$$\begin{aligned} B_{NL}^{(i)}(1,:) &= \frac{1}{2} \frac{\partial N_i}{\partial r} \left[\sum_{j=1}^8 u_j \frac{\partial N_j}{\partial r} \quad \sum_{j=1}^8 v_j \frac{\partial N_j}{\partial r} \quad \sum_{j=1}^8 w_j \frac{\partial N_j}{\partial r} \right] \\ B_{NL}^{(i)}(2,:) &= \frac{1}{2} \left[\sum_{j=1}^8 \frac{\partial N_i}{r \partial \theta} \left(u_j \frac{\partial N_j}{r \partial \theta} - 2v_j \frac{N_j}{r} \right) + \frac{N_i}{r} u_j \frac{N_j}{r} \quad \sum_{j=1}^8 \frac{\partial N_i}{r \partial \theta} \left(2u_j \frac{N_j}{r} + v_j \frac{\partial N_j}{r \partial \theta} \right) + \frac{N_i}{r} v_j \frac{N_j}{r} \quad \frac{\partial N_i}{r \partial \theta} \sum_{j=1}^8 w_j \frac{\partial N_j}{r \partial \theta} \right] \\ B_{NL}^{(i)}(3,:) &= \frac{1}{2} \frac{\partial N_i}{\partial z} \left[\sum_{j=1}^8 u_j \frac{\partial N_j}{\partial r} \quad \sum_{j=1}^8 v_j \frac{\partial N_j}{\partial r} \quad \sum_{j=1}^8 w_j \frac{\partial N_j}{\partial r} \right] \\ B_{NL}^{(i)}(4,:) &= \frac{\partial N_i}{\partial r} \left[\sum_{j=1}^8 u_j \frac{\partial N_j}{r \partial \theta} - v_j \frac{N_j}{r} \quad \sum_{j=1}^8 u_j \frac{N_j}{r} + v_j \frac{\partial N_j}{r \partial \theta} \quad \sum_{j=1}^8 w_j \frac{\partial N_j}{r \partial \theta} \right] \\ B_{NL}^{(i)}(5,1) &= \frac{\partial N_i}{\partial z} \left[\sum_{j=1}^8 u_j \frac{\partial N_j}{r \partial \theta} - v_j \frac{N_j}{r} \quad \sum_{j=1}^8 u_j \frac{N_j}{r} + v_j \frac{\partial N_j}{r \partial \theta} \quad \sum_{j=1}^8 w_j \frac{\partial N_j}{r \partial \theta} \right] \\ B_{NL}^{(i)}(6,:) &= \frac{\partial N_i}{\partial r} \left[\sum_{j=1}^8 u_j \frac{\partial N_j}{\partial z} \quad \sum_{j=1}^8 v_j \frac{\partial N_j}{\partial z} \quad \sum_{j=1}^8 w_j \frac{\partial N_j}{\partial z} \right] \end{aligned} \quad (20)$$

3.3 Stability equation

In this paper, buckling analysis is performed by obtaining sector stability equation which is based on resetting first and second changes of total sector potential energy to zero.

First, static balance relation is obtained using virtual work principal (first changes of total potential energy is zero). Total potential energy of the sector is as follows:

$$\Pi = U - W \quad (21)$$

where W includes the following external works:

$$W = W_b + W_s + W_p \quad (22)$$

$W_b + W_s$ and W_p are volume, surface, and centralized works of external forces, respectively. As we have ignored the weight of the sector in comparison with other loadings, only surface forces are not zero in the relation. Therefore, total external force work (which equals surface forces in this analysis) for each loading mode can be obtained.

Radial loading:

$$W = \left(\int_A \{\Delta\}^T [N_s]^T \{P\} dA \right)_{r=b,a} \quad (23a)$$

Circumferential loading:

$$W = \left(\int_A \{\Delta\}^T [N_s]^T \{P\} dA \right)_{\theta=0,\beta} \quad (23b)$$

Biaxial loading:

$$W = \left(\int_A \{\Delta\}^T [N_s]^T \{P\} dA \right)_{r=b,a} + \left(\int_A \{\Delta\}^T [N_s]^T \{P\} dA \right)_{\theta=0,\beta} \quad (23c)$$

In Eq. (25), $[N_s]$ is shape function matrix of nodes located on faces under loading. Strain-displacement relation is linear before buckling, thus strain energy of the sector is:

$$U = \frac{1}{2} \int_V \{\varepsilon_L\}^T \{\sigma\} dV \quad (24)$$

Replacing Eqs. (1) and (16) in (24), this relation can be expressed as:

$$U = \frac{1}{2} \int_V \{\Delta\}^T [B_L]^T [D][B_L] \{\Delta\} dV \quad (25)$$

Now, based on virtual work principal we have:

$$\delta\Pi = 0 \quad (26)$$

Choosing:

$$[K] = \int_V [B_L]^T [D][B_L] dV \quad (27)$$

$$\{F\} = \int_A [N_s]^T \{P\} dA \quad (28)$$

One can achieve static balance relation.

$$\{F\} = [K] \{\Delta\} \tag{29}$$

Displacement vector and consequently stress vector of each element can be obtained after forming elasticity matrix and force vector for each element. Next, second-order changes of total potential energy of the sector are reset to zero considering linear and nonlinear parts of strain-displacement relation to obtain stability equation.

$$\delta^2 \Pi = 0 \tag{30}$$

Second-order changes of external forces work and sector strain energy are:

$$\delta^2 W = 0 \tag{31}$$

$$\delta^2 U = \delta \{\Delta\}^T \int_V [B_L]^T [D] [B_L] dV \delta \{\Delta\} + \delta^2 U_{NL} \tag{32}$$

U_{NL} is potential energy at the moment of buckling.

$$U_{NL} = \frac{1}{2} \int_V \{\varepsilon_{NL}\}^T [\sigma^0] dV \tag{33}$$

Replacing Eqs. (2) and (7) in (33), Eq. (33) can be rewritten in matrix form.

$$U_{NL} = \frac{1}{4} \int_V \{\Delta\}^T [G]^T [S] [G] \{\Delta\} dV \tag{34}$$

$$[G] = \begin{bmatrix} \frac{\partial N_1}{\partial r} & 0 & 0 & \frac{\partial N_8}{\partial r} & 0 & 0 \\ \frac{\partial N_1}{r \partial \theta} & -\frac{N_1}{r} & 0 & \frac{\partial N_8}{r \partial \theta} & -\frac{N_8}{r} & 0 \\ \frac{\partial N_1}{\partial z} & 0 & 0 & \frac{\partial N_8}{\partial z} & 0 & 0 \\ 0 & \frac{\partial N_1}{\partial r} & 0 & 0 & \frac{\partial N_8}{\partial r} & 0 \\ \frac{N_1}{r} & \frac{\partial N_1}{r \partial \theta} & 0 & \dots & \frac{N_8}{r} & \frac{\partial N_8}{r \partial \theta} & 0 \\ 0 & \frac{\partial N_1}{\partial z} & 0 & 0 & \frac{\partial N_8}{\partial z} & 0 \\ 0 & 0 & \frac{\partial N_1}{\partial r} & 0 & 0 & \frac{\partial N_8}{\partial r} \\ 0 & 0 & \frac{\partial N_1}{r \partial \theta} & 0 & 0 & \frac{\partial N_8}{r \partial \theta} \\ 0 & 0 & \frac{\partial N_1}{\partial z} & 0 & 0 & \frac{\partial N_8}{\partial z} \end{bmatrix} \tag{35}$$

$$[S] = \begin{bmatrix} [\sigma^0] & [0] & [0] \\ & [\sigma^0] & [0] \\ \text{sym.} & & [\sigma^0] \end{bmatrix} \tag{36}$$

Replacing Eqs. (31) and (32) in Eq. (30) and choosing:

$$[K_G] = \int_V [G]^T [S] [G] dV \tag{37}$$

Stability equation of buckling can be written as follows:

$$([K] + [K_G]) \delta \{\Delta\} = 0 \tag{38}$$

4 RESULTS AND VERIFICATION

4.1 Verification of the results

To study the accuracy of results extracted from written code, first the convergence of the obtained results is examined. In this analysis, 3D 8-noded elements are used. Fig. 3 shows an example of load convergence leading to buckling for a non-perforated sector with geometric dimensions of $b = 0.5 [m], a = 1 [m], h = 0.025 [m]$ and $\beta = 90^\circ$ which are under combined loading (biaxial) and convergence of results increases as the number of elements rises.

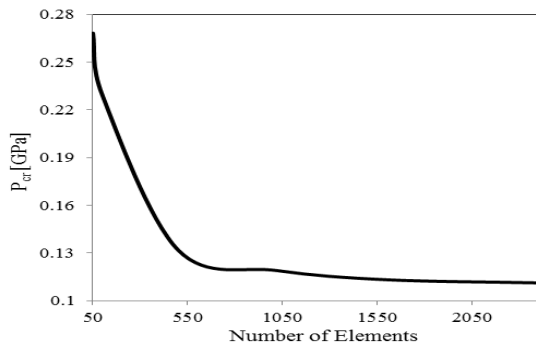


Fig.3
Mechanical buckling stress vs. number of elements.

Next step is validating the results. As there is no mechanical buckling load analysis for perforated composite sector plates, validations is performed based on the results of [14] for homogenous sector without opening and with geometric dimensions of $b = 0.5 [m], a = 1 [m], h = 0.05 [m]$ and $\beta = 60^\circ$ which is made of pure ceramic (Zirconia, ZrO_2) with engineering characteristics of $E = 151 [GPa]$ and $\nu = 0.3$ (Table 4).

Table 4
Mechanical buckling stress [GPa] for ceramic annular sector plate.

Loading direction	Present	Ref. [14]
Radial	2.3761	2.3400
Circumferential	9.3378	9.2000
Biaxial	2.2565	2.2200

Reference [14] is used from finite element method based on 3-D elasticity, too; but instead of using continuous functions for material properties, used from shape functions. (Using graded element has computing error.)

4.2 Results

In all of the cases inner and outer radius is $0.5[m]$ and $1[m]$, respectively. Angles of sector is $\beta = 60, \beta = 90$. Also the thickness of sector is selected $0.025[m]$, $0.05[m]$.

Table 5. shows the results of mechanical load leading to buckling for perforated sector with internal diameter of $0.5[m]$, external diameter of $1[m]$ and cutout radial variations of 12° for sector 60° and 18° for sector 90° . Critical load for two thicknesses of $0.025[m]$ and $0.05[m]$ are reported which this plate with thickness of $0.05[m]$ and dimensions of $b = 0.5 [m]$ and $a = 1 [m]$ can be placed in thick plate range regarding existing theories of plate. As it is shown, when dimensions are specified, as the thickness of the sector is reduced, the fewer loads is needed for buckling to occur due to reduced elasticity and vice versa. According to results, plate under combined loading has lower strength compared with radial loading. In addition, plate strength against radial loading is less than circumferential loading. Sector plate geometry is the reason of great numbers affected by circumferential loading which buckling occurs later in this mode. Results of two angles of 60° and 90° in the sector shows that the less the angle of the sector is, the longer it takes for buckling to occur in the plates which is under radial and combined loading mode; but, reducing the angle of sector leads to buckling with smaller load in the directions of circumferential loading due to approaching of two lateral surfaces (right and left faces).

Table 5
Mechanical buckling stress [GPa] for sector plate with bean shape cut-out with $r_2 - r_1 = (a - b) / 5 = 0.1 [m], \theta_2 - \theta_1 = \beta / 5$.

Loading direction	[0,90] ₄				[45,-45] ₄			
	$h=0.025[m]$	$h=0.05[m]$	$h=0.025[m]$	$h=0.05[m]$	$h=0.025[m]$	$h=0.05[m]$	$h=0.025[m]$	$h=0.05[m]$
	$\beta=60^\circ$	$\beta=90^\circ$	$\beta=60^\circ$	$\beta=90^\circ$	$\beta=60^\circ$	$\beta=90^\circ$	$\beta=60^\circ$	$\beta=90^\circ$
Radial	0.2202	0.1134	0.6447	0.3674	0.1966	0.1060	0.5878	0.3390
Circumferential	0.7019	0.7884	1.6451	1.6817	0.7062	1.0341	1.6855	2.2457
Biaxial	0.1235	0.0839	0.4220	0.2898	0.1131	0.0936	0.3994	0.3207

Table 6. presents results of mechanical buckling load on perforated sector with internal and external diameter of $0.5[m]$ and $1[m]$ respectively, cutout radial variations of $1[m]$ and cutout circumferential variations of 20° for 60° sector and 30° for 90° sector. Circumferential loading makes sector plate buckles later than radial loading due to its geometry and later buckling is radial loading expected compared with combined loading. Reducing the gradient of the sector leads to large buckling load under radial and combined loading and fewer buckling load is obtained under circumferential loading.

Comparing two arrangements shows that stacking sequence [0,90]₄ under radial loading leads to more buckling load than stacking sequence [45,-45]₄ but critical load will be fewer under circumferential loading.

Table 6
Mechanical buckling stress [GPa] for sector plate with bean shape cut-out with $r_2 - r_1 = (a - b) / 5 = 0.1 [m], \theta_2 - \theta_1 = \beta / 3$.

Loading direction	[0,90] ₄				[45,-45] ₄			
	$h=0.025[m]$	$h=0.05[m]$	$h=0.025[m]$	$h=0.05[m]$	$h=0.025[m]$	$h=0.05[m]$	$h=0.025[m]$	$h=0.05[m]$
	$\beta=60^\circ$	$\beta=90^\circ$	$\beta=60^\circ$	$\beta=90^\circ$	$\beta=60^\circ$	$\beta=90^\circ$	$\beta=60^\circ$	$\beta=90^\circ$
Radial	0.1983	0.0975	0.6043	0.3080	0.2003	0.0952	0.5522	0.2979
Circumferential	0.6651	0.8161	1.4426	1.7991	0.6678	1.0286	1.5873	2.2775
Biaxial	0.1065	0.0659	0.3756	0.2254	0.1081	0.0774	0.3613	0.2686

Table 7. shows critical load of mechanical buckling for perforated sector with internal and external diameters of $0.5[m]$ and $1[m]$, respectively, cutout radial variations of $0.1667[m]$ and cutout circumferential variations of 12° for 60° sector and of 18° for 90° sector.

Based on the results for buckling of the sector plate in sectors with different cutout, by increasing the size of cut out, the strength will be lower under radial and combined loading; but, sometimes the cutout leads to the improvement of buckling behavior in the plate under circumferential loading.

Table 7

Mechanical buckling stress [GPa] for sector plate with bean shape cut-out with $b = 0.5 [m], a = 1 [m], r_2 - r_1 = (a - b) / 3 = 0.1667 [m], \theta_2 - \theta_1 = \beta / 5$.

Loading direction	[0,90] ₄				[45,-45] ₄			
	$h=0.025[m]$	$h=0.05[m]$	$h=0.025[m]$	$h=0.05[m]$	$h=0.025[m]$	$h=0.05[m]$	$h=0.025[m]$	$h=0.05[m]$
	$\beta=60^\circ$	$\beta=90^\circ$	$\beta=60^\circ$	$\beta=90^\circ$	$\beta=60^\circ$	$\beta=90^\circ$	$\beta=60^\circ$	$\beta=90^\circ$
Radial	0.1988	0.1023	0.5770	0.3315	0.1772	0.0938	0.5556	0.3022
Circumferential	0.6784	0.7511	1.6284	1.7078	0.7290	0.9516	1.7321	2.1746
Biaxial	0.1059	0.0746	0.3668	0.2549	0.1014	0.0828	0.3563	0.2832

Table 8. shows mechanical buckling load of perforated sector with internal and external diameters of $0.5 [m]$ and $1 [m]$, respectively, cutout radial variations of $0.1667 [m]$ and cutout circumferential variations of 20° for 60° sector and of 30° for 90° sector. Cutout dimensions can be increased for obtaining higher buckling strength if sector is under circumferential loading. For a sector with above dimensions, doubling the thickness with other specified dimensions leads to more than two- fold increase of buckling strength of sector plate compared with the initial state.

Table 8

Mechanical buckling stress [GPa] for sector plate with bean shape cut-out with $r_2 - r_1 = (a - b) / 3 = 0.1667 [m], \theta_2 - \theta_1 = \beta / 3$.

Loading direction	[0,90] ₄				[45,-45] ₄			
	$h=0.025[m]$	$h=0.05[m]$	$h=0.025[m]$	$h=0.05[m]$	$h=0.025[m]$	$h=0.05[m]$	$h=0.025[m]$	$h=0.05[m]$
	$\beta=60^\circ$	$\beta=90^\circ$	$\beta=60^\circ$	$\beta=90^\circ$	$\beta=60^\circ$	$\beta=90^\circ$	$\beta=60^\circ$	$\beta=90^\circ$
Radial	0.1810	0.0900	0.5132	0.2706	0.1844	0.0871	0.5091	0.2692
Circumferential	0.6428	0.7324	1.4442	1.6067	0.6638	0.9102	1.5582	2.0584
Biaxial	0.0914	0.0581	0.3016	0.1940	0.0957	0.0713	0.3195	0.2424

5 CONCLUSIONS

In this paper, 3D elasticity relation and finite element method was used to study the load leading to the buckling of composite sector plate with bean-shaped cutout in different conditions and the effect of loading direction, layer arrangement, cutout and sector dimensions on buckling strength of the plate was examined.

- Results show that buckling of the plate for any dimensions of the cutout or the sector is larger under circumferential loading than radial loading and it is also larger under radial than combined loadings.
- In all geometric conditions of perforated sector with different stacking sequence, load leading to buckling under radial and combined loading is larger for a 60° sector than 90° one but buckling load under circumferential loading is smaller for 60° sector than 90° one which is because of sector geometry and more elasticity in smaller gradients of the sector.
- In sector plates with different cutout dimensions, loading direction and stacking sequence, the thicker plate is more loads needed until buckling occurs.
- According to the extracted results, increasing the dimensions of the cutout leads to reduction in the buckling strength of the sector plate in radial and combined loading directions but the existence of cutout for circumferential loading may sometimes lead to increase or decrease of sector buckling strength.

Finally, it can be said that based on loading, critical load leading to buckling can be controlled by correct selection of stacking sequence and sector and cutout dimensions if it is needed to use perforated composite sector plate.

REFERENCES

- [1] Bruno D., Lato S., 1991, Buckling of moderately thick composite plates, *Journal of Computers & Structures* **18**: 65-75.
- [2] Chai G. B., 1994, Buckling of generally laminated composite plates with various edge support conditions, *Journal of Composite Structures* **29**: 299-310.
- [3] Kim Y. S., Hoa S. V., 1995, Bi-axial buckling behavior of composite rectangular plates, *Journal of Composite Structures* **31**: 247-252.
- [4] Zhou Y. H., Zheng X., Harik I. E., 1995, A Semi-numerical method for buckling of sector plates, *Journal of Computers & Structures* **57**(5): 847-854.

- [5] Sundaresan P., Singh G., Rao V., 1998, Buckling of moderately thick rectangular composite plates subjected to partial edge compression, *Journal of Mechanical Sciences* **40**(11): 1105-1117.
- [6] Shariyat M., 2007, Thermal buckling analysis of rectangular composite plates with temperature-dependent properties based on a layer wise theory, *Journal of Thin-Walled Structures* **45**: 439-452.
- [7] Özben T., 2009, Analysis of critical buckling load of laminated composites plate with different boundary conditions using FEM and analytical methods, *Journal of Computational Materials Science* **45**: 1006-1015.
- [8] Alipour M. M., Shariyat M., 2011, Semi-analytical buckling analysis of heterogeneous variable thickness viscoelastic circular plates on elastic foundations, *Journal of Mechanics Research Communications* **38**: 594-601.
- [9] Dash P., Singh B. N., 2012, Buckling and post-buckling of laminated composite plates, *Journal of Mechanics Research Communications* **46**: 1-7.
- [10] Jabbarzadeh M., Baghdar M.K. D., 2013, Thermal buckling analysis of FGM sector plates using differential quadrature method, *Journal of Modares Mechanical Engineering* **13**(2): 33-45.
- [11] Asemi K., Shariyat M., 2013, Highly accurate nonlinear three-dimensional finite element elasticity approach for biaxial buckling of rectangular anisotropic FGM plates with general orthotropy directions, *Journal of Composite Structures* **106**: 235-249.
- [12] Fazzolari F.A., Banerjee J. R., Boscolo M., 2013, Buckling of composite plate assemblies using higher order shear deformation theory-An exact method of solution, *Journal of Thin-Walled Structures* **71**: 18-34.
- [13] Lopatin A.V., Morozov E.V., 2014, Buckling of a uniformly compressed composite rectangular CCCC sandwich plate, *Journal of Composite Structures* **108**: 332-340.
- [14] Asemi K., Salehi M., Akhlaghi M., 2014, Post-buckling analysis of FGM annular sector plates based on three dimensional elasticity graded finite elements, *Journal of Non-Linear Mechanics* **67**: 164-177.
- [15] Abolghasemi S., Shaterzadeh A.R., Rezaei R., 2014, Thermo-mechanical buckling analysis of functionally graded plates with an elliptic cutout, *Journal of Aerospace Science and Technology* **39**: 250-259.
- [16] Nasirmanesh A., Mohammadi S., 2015, XFEM buckling analysis of cracked composite plates, *Journal of Composite Structures* **131**: 333-343.
- [17] Rezaei R., Shaterzadeh A.R., Abolghasemi S., 2015, Buckling analysis of rectangular functionally graded plates with an elliptic hole under thermal loads, *Journal of Solid Mechanics* **7**(1): 41-57.
- [18] Shaterzadeh A. R., 2015, Thermo-mechanical buckling analysis of FGM plates with circular cut out, *Journal of Solid and Fluid Mechanics* **5**(2): 97-107.
- [19] Mansouri M. H., Shariyat M., 2015, Biaxial thermo-mechanical buckling of orthotropic auxetic FGM plates with temperature and moisture dependent material properties on elastic foundations, *Journal of Composites Part B* **83**: 88-104.
- [20] Asemi K., Shariyat M., Salehi M., Ashrafi H., 2013, A full compatible three-dimensional elasticity element for buckling analysis of FGM rectangular plates subjected to various combinations of biaxial normal and shear loads, *Journal of Finite Elements in Analysis and Design* **74**: 9-21.
- [21] Herakovitch C. T., 1998, *Mechanics of Fibrous Composites*, 1st Edition, Amazon.
- [22] Zienkiewicz O. C., Taylor R. L., 2000, *The Finite Element Method: It's The Basis*, 5th Edition, Amazon.
- [23] Darvizeh M., Darvizeh A., Shaterzadeh A.R., Ansari R., 2010, Thermal buckling of spherical shells with cut-out, *Journal of Thermal Stresses* **33**: 441-458.